Chapter 7

MODEL DEVELOPMENT IV

Application to full-scale

Considered in this chapter is the final phase of model development - the application of the new keel load model for vertical structures to full-scale. The influence of interaction speed which has fluid dynamic and global inertia consequences is discussed theoretically and suggestions for modelling are given. A trial sensitivity study of the new model at full-scale is then described. Performance is compared to other models in the literature. Until now, only laboratory data have been used for model development and calibration, primarily because of the scarcity of field data. In this chapter the full-scale ridge factor and line load data from Section 2.3 are revisited and the results of the thesis model sensitivity study are reviewed in light of this information.

7.1 Fluid dynamic considerations

In Section 5.1 it was suggested that the acceleration of fluid around a structure in steady state flow may affect ice block stability. Also, blocks and ice debris uplifted in the early stages of an interaction may not settle soon enough to create a surcharge. This argument is further developed in this section.

Suspension of a block

The suspension of an ice block from the surface of a ridge keel may be caused by fluid rushing out of a compressed zone, or fluid rushing past the surface. The total force

required to accelerate a body through a fluid is the sum of the fluid resistance forces (drag and inertia) plus the inertia force of the body (mass times acceleration). In the case of a rubble block roughly circular in shape, square-edged and oriented perpendicular to the direction of acceleration, it can be shown (Sarpkaya and Garrison, 1982, Bruneau, 1992) that the force required to accelerate such a body is

$$F(t) = \frac{1}{2}\rho(\pi r_a^2)V(t)^2 C_d + (M_b + (\frac{8}{3}\rho r_a^3))\frac{dV}{dt}C_m \qquad (88)$$

where r_a is the radius of the block, M_b is the mass of the block, $V(t)$ is instantaneous speed and C_d and C_m represent the drag and inertia coefficients for uniformly accelerated flow.

A stationary body perpendicular to flow may be suspended in a surrounding fluid if the flow rate exceeds a critical velocity. The critical velocity in the case of a rubble block may be equated to the terminal velocity which is determined by ignoring the inertia term above (in Equation 88) and equating the drag term to body weight. Thus for a block of ice 1 m in diameter and 0.2 m thick, suspension occurs when axial flow velocity reaches 0.58 m/s (when $C_d = 1.15$, $\rho_i = 910$ kg/m^3, $\rho_w = 1010$ kg/m^3). In air, the terminal velocity for the same block would be 50 m/s ($\rho_{air} = 1.25$ kg/m^3) which underscores the near weightlessness of ice under water.

For a block lying flat, suction forces may be considered. According to Bernoulli's equation, the term $[\rho V^2/2 + P]$ is constant where P is the ambient pressure. If it is assumed that the fluid flow is zero on one side of the block and equal to V on the other, then the uplift pressure is equal to the $\rho V^2/2$ (dynamic pressure) term. For the submerged

submerged block (1 m diameter, 0.2 m thick), the speed required for uplift is approximately 0.55 m/s. This number is close to the suspension or terminal velocity computed above, so it unlikely that a block lifted under these circumstances would settle very soon.

Velocity field around cylinder

The velocity field around a circular cylinder may be determined for incompressible potential flow from a closed form solution of Navier-Stokes equation. The longitudinal, u, and lateral, v, velocity components as shown in Figure 7.1 are defined by

$$u = -U_o\left[\frac{r_a^2}{R^2}\cos 2\theta - 1\right] \quad ; \quad v = -U_o\frac{r_a^2}{R^2}\sin 2\theta \tag{89}$$

where U_o is the far field relative velocity, r_a is the radius of the cylinder, and R and θ are the radial and angular distance to the point of interest (Davenport, 1989). The maximum velocity is $2U_o$ and occurs on the sides of the cylinder at $\theta = 90°$ and 270° where pressure is also a minimum. The maximum lateral velocity is equivalent to the far field velocity ($v_{max} = U_o$) and occurs at $\theta = \pm 45°$, $\pm 135°$. Typically, flow separates and boundary layers are present so flow is not potential, however, upstream (approximately the front half of the cylinder) where separation does not occur the approximation of potential flow is a good one.

Keel interaction dynamics

It has been shown that a body in a fluid may be suspended through the action of drag and suction. We have also seen that fluid accelerates around a cylinder reaching a peak lateral speed equal to the approach speed and doubling the longitudinal speeds around the

structure sides. It is assumed here that blocks at rest on the surface of a ridge keel are engaged with one another as a result of buoyant and cohesive forces (assuming that friction is essentially absent at the surface). Two cases are now considered: in the first a 1 m diameter circular block is projected half way out of a frictionless planar keel surface approaching a large cylindrical structure, in the second, a similar block lies flat on the keel surface (Figure 7.2).

When an interaction commences consider the fluid at $\theta = 135°$ and 225° (Figure 7.1) near the structure where the lateral fluid speed is a maximum (U_o), acceleration is zero and thus the fluid dynamic forces result from drag and suction. If we consider bulk cohesion to act evenly over all block surfaces it can be shown that cohesion must exceed 450 Pa to avoid uplift of the prostrate block due to suction if U_o is 1 m/s. For the upright block if bulk cohesion alone were holding it in place (on one side) then it would have to exceed 580 Pa. As the region in which these blocks are located approaches the surface of the structure near the sides the "absolute" speed almost doubles. Ignoring inertia momentarily, this would increase the drag and uplift forces by a factor of four. It is entirely possible that in a natural first-year ridge keel a block may be inclined so as to produce some added lift component as well which would further upset the equilibrium of forces holding the block in place.

Though approximate and highly idealized, the scenarios in the preceding review demonstrate the sensitivity of keel ice block stability to interaction speeds and the importance of cohesion at the keel surface. There are other fluid dynamic factors which must also be considered during interactions. Of particular interest are fluid dynamic and body inertia forces.

Inertia considerations

If a large mass of rubble, such as a "plug", were displaced from rest in a stationary fluid it can be shown that substitution of the relative body parameters (effective dimensions, coefficients, etc.) into Equation (88) yields the total inertia and drag force on that body. In soil mechanics an inertia term analogous to that above has been formulated for the horizontal inertia of displaced soil in front of an advancing tine:

$$F_i = \rho D_f H_f V^2 \frac{\sin\alpha \cos(45-\phi/2)}{\sin(\alpha+45-\phi/2)} \qquad (90)$$

where ρ is the density of the material displaced, α is the rake angle (to forward horizontal), D_f is effective width over the furrow depth, H_f, V is the speed and ϕ is the internal friction angle of the soil (Stafford, 1984).

It would be quite easy to apply a "plug" inertia factor like these to ridge failure forces but it may not be correct to do so. Though increased interaction speed is associated with increased accelerations causing inertial forces it also diminishes block engagement pressures as described earlier. Figure 7.3 illustrates the competing force processes on a ridge keel interacting with a structure. Though the position and relative strength of individual curves is somewhat arbitrary it is entirely possible that the net speed effect is near zero as shown. This is supported in the laboratory by the results reported in Chapter 3, the regression results of Chapter 4 and the detailed analysis in Chapter 6. Not shown in the figure are the effects of alternate failure modes or simply the adjustment of the assumed failure shape that would likely result from significant speed changes. This brief study does not provide closure to this topic but speed effects will not be considered further here. This will likely be a fruitful area of research for future analytical work.

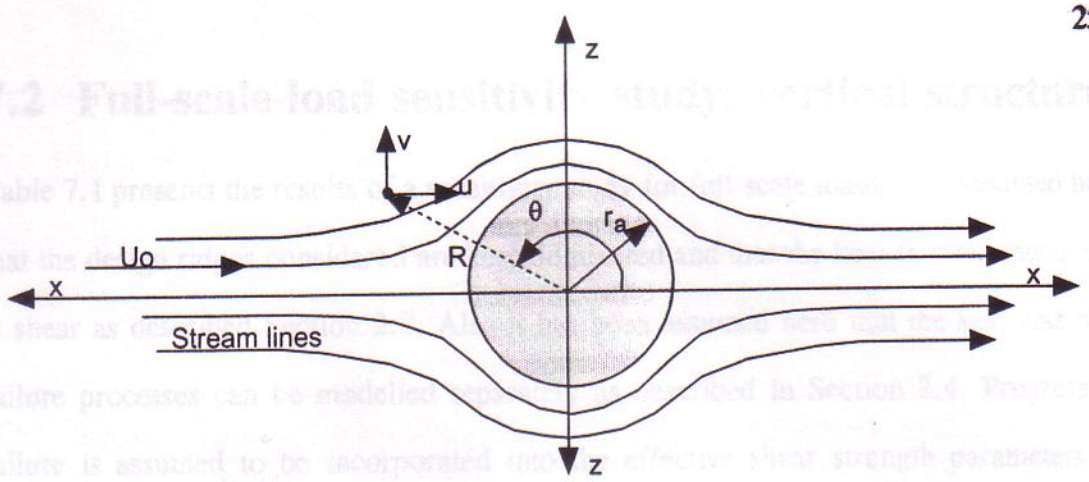

Figure 7.1 Potential flow around a cylinder.

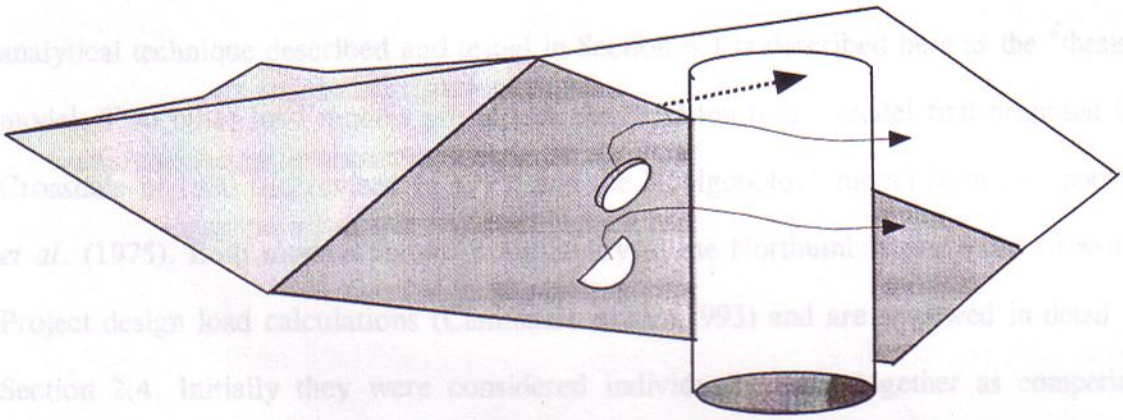

Figure 7.2 Keel block suspension scenarios.

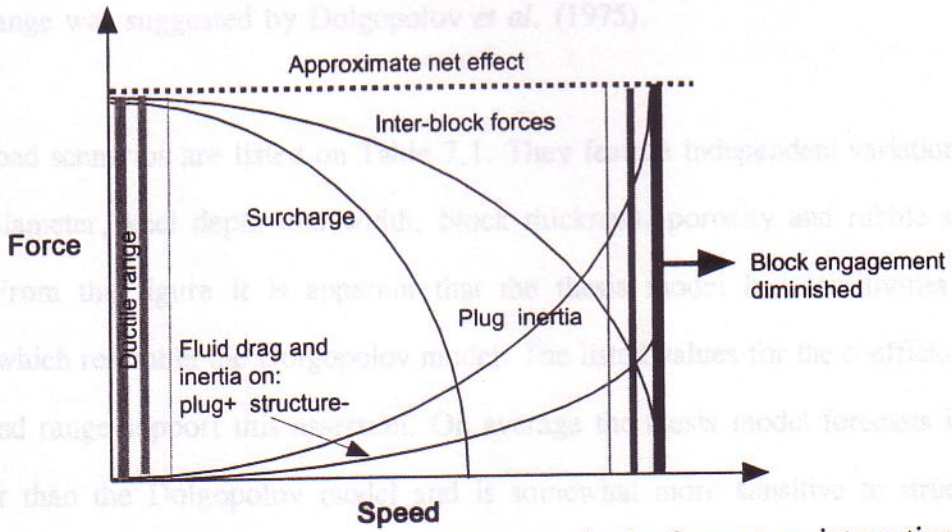

Figure 7.3 Competing fluid dynamic force processes for keel-structure interactions.

7.2 Full-scale load sensitivity study: vertical structures

Table 7.1 presents the results of a sensitivity study for full-scale loads. It is assumed here that the design ridges considered are keel-dominated and that the keel failure mechanism is shear as described Section 2.2. Also it has been assumed here that the keel and core failure processes can be modelled separately as described in Section 2.4. Progressive failure is assumed to be incorporated into the effective shear strength parameters as discussed in Section 6.1. Default values for the ridge geometry and properties are somewhat representative of design conditions for the Northumberland Strait. The analytical technique described and tested in Section 6.1 is described here as the "thesis" model. Two other load models are tested: the "friction plug" model first proposed by Croasdale in 1980 and revised in 1994, and the "Dolgopolov" model from Dolgopolov *et al.* (1975). Both models feature prominently in the Northumberland Strait Crossing Project design load calculations (Cammaert *et al.* (1993) and are reviewed in detail in Section 2.4. Initially they were considered individually, then together as competing mechanisms in the so-called *cross-over* technique. Note that, as in the thesis model, there is no assumed accumulation of displaced rubble (surcharge) in the Dolgopolov model, though a range was suggested by Dolgopolov *et al.* (1975).

Fourteen load scenarios are listed on Table 7.1. They feature independent variations of structure diameter, keel depth and width, block thickness, porosity and rubble shear strength. From the figure it is apparent that the thesis model has sensitivities and responses which resemble the Dolgopolov model. The listed values for the coefficient of variance and range support this assertion. On average the thesis model forecasts loads 15% lower than the Dolgopolov model and is somewhat more sensitive to structure

diameter, less sensitive to keel depth and is uniquely sensitive to changes in ridge width. The friction plug model predicts loads which are on average 36% of the thesis model values. The form of the plug model selected has no cohesion term which eliminates related responses and significantly affects the coefficient of variation for model output.

To compare the results of this sensitivity analysis to the model sensitivity study in Section 2.4, Scenario 4 on Table 7.1 is considered. This scenario is chosen because it is the only one that matches the "default" conditions of all the models reviewed in Figure 2.15, including the values quoted for the numerical simulations by Brown and Bruce (1995) and Sayed (1995). Remarkably, the average default value for all these models was 6.5 MN which is equivalent to the load predicted here by the thesis model. This unwitting endorsement by a broad range of experts strengthens the relevancy of the model.

There are a few distinct advantages to the thesis model over the others reviewed in this study. The thesis model demonstrates a sensitivity to ridge width which is not realized in the Dolgopolov model unless it is analytically "truncated" via plug shear models or otherwise. The model also utilizes an assumed shape for ridge keels which better approximates natural ridges than other modelling approaches. Surcharge effects are implicit in the thesis model whereas a broad range of possible values are suggested for the other models. Also in the thesis model an empirical effective structure width formula is used. Most importantly, the thesis model is based on fundamental equilibrium mechanics, uses regression equations based on a broad range of new and old data, and has demonstrated a high degree of success predicting forces in the laboratory. To examine sensitivity results further, the next section revisits full-scale load data from Chapter 2.

Table 7.1 Sensitivity analysis of thesis model at full-scale.

	Scenario	Diameter D (m)	Depth H (m)	Width* W (m)	Block thick Li (m)	Porosity e (%)	Friction** ϕ (deg)	Coh.*** c (Pa)	Thesis mod. Force MN	Fric plug**** Force MN	Dolgop.***** Force MN
1	"Default settings"	10	15	47.4	0.2	35	15.57	3241	4.30	1.26	5.05
2	Diameter Increased	15	15	47.4	0.2	35	15.57	3241	6.16	1.58	6.31
3	Diameter decreased	5	15	47.4	0.2	35	15.57	3241	2.33	0.95	3.79
4	Depth increased	10	20	60.0	0.2	35	15.57	3241	6.52	2.49	9.14
5	Depth decreased	10	10	34.7	0.2	35	15.57	3241	2.50	0.51	2.34
6	Width increased	10	15	100.0	0.2	35	15.57	3241	5.49	2.67	5.05
7	Block thickness increased	10	15	47.4	0.3	35	0	4866	3.67	0.00	4.35
8	Block thickness decreased	10	15	47.4	0.1	35	32.37	1617	5.10	2.87	6.51
9	Porosity increased	10	15	47.4	0.2	45	29.27	3241	6.01	2.15	6.86
10	Porosity decreased	10	15	47.4	0.2	25	1.87	3241	3.10	0.17	3.78
11	Average shear (all labs)	10	15	47.4	0.2	35	31	588	3.62	2.72	5.11
12	Sample friction only	10	15	47.4	0.2	35	45	0	6.00	4.53	8.36
13	Sample cohesion only	10	15	47.4	0.2	35	0	5000	3.75	0.00	4.43
14	Sample friction and cohesion	10	15	47.4	0.2	35	45	5000	14.58	4.53	15.60
	Average								**5.22**	**1.89**	**6.19**
	Stan Dev.								**2.92**	**1.46**	**3.15**
	C.O.V								**0.56**	**0.78**	**0.51**
	Min								**2.33**	**0.00**	**2.34**
	Max								**14.58**	**4.53**	**15.60**
	Range								**12.25**	**4.53**	**13.26**

Notes: * Ridge width is computed in all scenarios except 6 from Section 2.1: W = 2.53H+9.4
** Friction angle is computed for scenarios 1 - 10 from Section 4.1: ϕ = 1.22 - 168Li + 1.37e
*** Cohesion is computed in scenarios 1 - 10 from Section 4.1: c = 16240Li - 7
**** Frictional plug model as per section 2.1 Croasdale (1994)
***** Dolgopolov et al (1975) model as per Section 2.1 - no surcharge, w/ shape factor

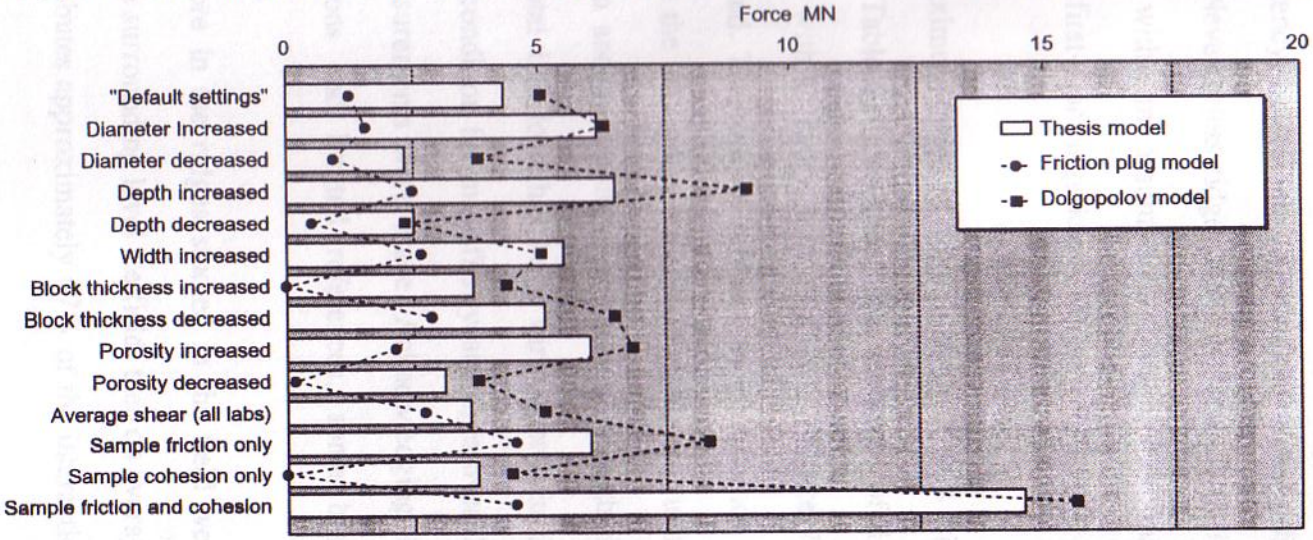

7.3 Discussion of full-scale loads

As described in subsection 2.3.1 the value of a ridge factor as a design tool is significantly compromised by the unknown state of the refrozen core in a first-year ridge. Without any knowledge of the core competency the relative contributions of the ridge elements cannot be accurately determined. Nevertheless ridge factors do provide useful guidelines for bounding load estimates, and, with some assumptions about the core, may reveal approximate average load values for first-year ridge keels.

The information in Table 2.4 indicated a maximum range of ridge factors of 1 to 4 with an average of 2.3 for the references cited. Table 2.4 also shows that the range of line loads is 500 to 1024 kN/m (where quoted) with an average of 800 kN/m. Figure 7.4 shows how these values have been interpreted. The ratio of refrozen core resistance to level ice resistance has been plotted against the maximum, mean and minimum rubble line loads for each of the maximum, mean and minimum ridge factors. Though the contribution of the refrozen core to the total line load has been varied between the maximum limits, this probably exceeds the condition for most first-year ridges over the period in which it is likely that force measurements were made. Acknowledging the varied structural geometries, ice conditions and limited references, some basic observations may be drawn from the figure.

- If one assumes that the refrozen core in the ridges studied in the field were approximately equal in strength to the surrounding level ice field, then on average the rubble portion of the ridge contributes approximately 57% of the interaction force or 450 kN/m.
- If a ridge had a core which generated twice the resistance of the surrounding level

ice then, on average, the rubble line load would be closer to 100 kN/m.

- If there were no core present or if it did not provide any significant resistance then the average rubble line load would be 800 kN/m, and the upper and lower line load limits would be approximately 1000 kN/m and 500 kN/m respectively.

For a 10 m wide structure, the forces due to rubble would vary from 1 to approximately 10 MN for the cases considered above. If the refrozen core and level ice are equal in resistance then, for the average condition in which the ridge factor is 2.3 and the line load is 800 kN/m, the force on a 10 m wide structure would be 4.5 MN.

A highly favourable condition arises when the results from the sensitivity study in section 7.2 are considered in light of the results in Figure 7.4. Figure 7.5 shows the sensitivity study results for the thesis model superimposed on the ridge factor study. The mean and standard deviation line loads from the sensitivity study are shown as horizontal parallel lines. The shaded region outlines the entire range of outcomes from the ridge factor study with the darker intensity indicating a higher probability of occurrence.

The ratio of refrozen core resistance (including sail effects) to level ice resistance with the highest probability of occurrence is assumed here to be 1. This value is representative, at some time, of all ridges with cores which become thicker and stronger than level ice. For these ridges, which may also be keel-dominated, the insulation effects of snow and ice restrict rapid core growth and warm that which does form. Also, the downward growth of a refrozen layer through a random rubble matrix results in a highly variable core thickness. This condition may reduce the strength of a thickened core since the weakest parts will attract failure and possibly alter failure modes. A core ratio less than 1 is also possible since those design ridges which have been shown under some

conditions (NSCP) to be keel-dominated may have no core at all. Since the ridge factor data are for a broad range of structure geometries and ice conditions, the core failure mode may vary appreciably. Thus considering the ranges of age, geometry and failure mode for those ridges measured, an average core resistance ratio of 1 has been assumed.

A dashed white ellipse marks the region surrounding the mean ridge factor and mean line load - centred on the darkest shaded region corresponding to a core resistance ratio of 1. As can be seen in the figure the line which marks the mean thesis model line load from the sensitivity study almost bisects the ellipse. Furthermore, the point of intersection between this line and that for the mean ridge factor and line load is well within the region of high occurrence probability for full-scale loads. The sensitivity study line load is slightly greater (14%) than that which has been calculated as the average for full-scale loads. This study shows that the thesis model results are highly consistent with the full-scale load data available.

As demonstrated here and in Section 6.1 the proposed analytical model was unable to precisely match laboratory ice rubble experiments. The errors introduced through measurement and analysis are only partially responsible. Underlying many processes is a natural variability that is, and will remain, beyond reasonable deterministic modelling capabilities. Recognising this, probabilistic modelling techniques have been developed and are now an integral part of most load forecasting projects. Like others, the thesis model is closed-form and may conveniently be incorporated into probabilistic modelling algorithms. There, distributions replace specific values for input parameters and random sampling simulations or distribution manipulation techniques provide return period load estimates for risk analysis.

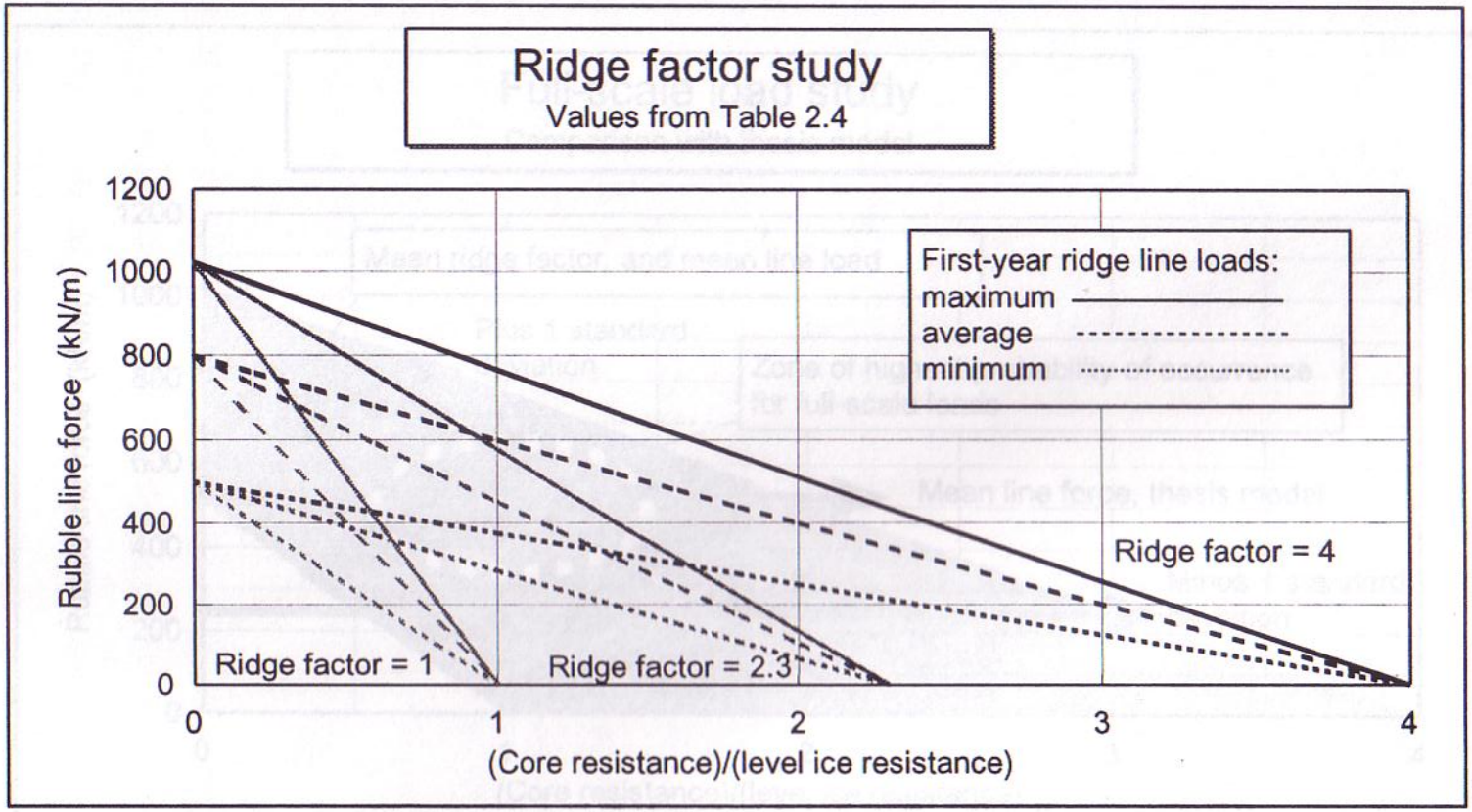

Figure 7.4 Interpretation of full-scale load data.

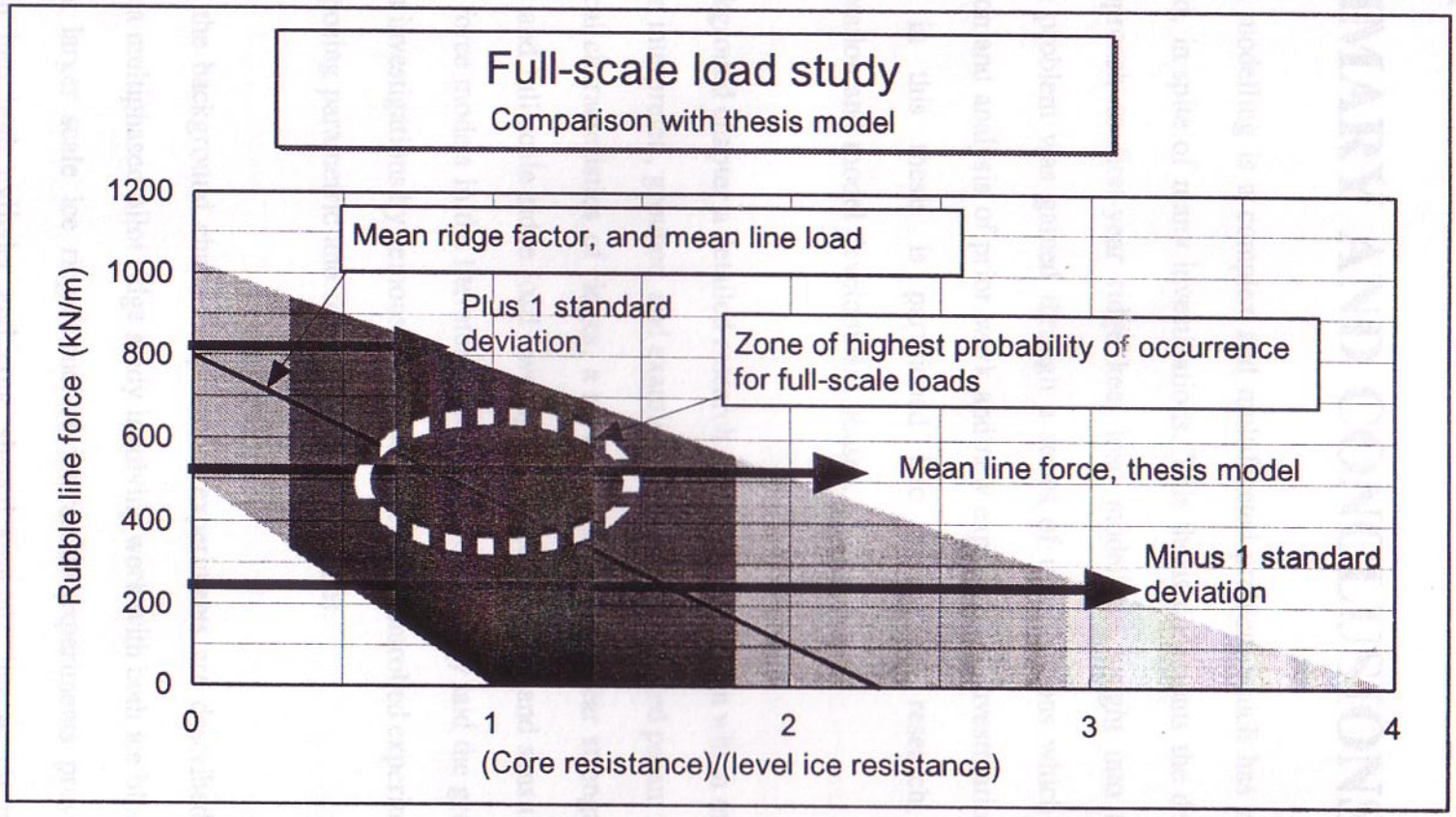

Figure 7.5 Comparison of full-scale data with the thesis model sensitivity study.